HAL
open science

# Vertical breakdown of GaN on Si due to V-pits

S. Besendörfer, E. Meissner, A. Tajalli, M. Meneghini, J. Freitas, J. Derluyn, F Medjdoub, G. Meneghesso, J. Friedrich, T. Erlbacher

## To cite this version:

S. Besendörfer, E. Meissner, A. Tajalli, M. Meneghini, J. Freitas, et al.. Vertical breakdown of GaN on Si due to V-pits. Journal of Applied Physics, 2020, 127 (1), pp.015701. 10.1063/1.5129248 . hal-02429980

**HAL Id: hal-02429980**

**https://hal.science/hal-02429980v1**

Submitted on 1 Dec 2020

**HAL** is a multi-disciplinary open access archive for the deposit and dissemination of scientific research documents, whether they are published or not. The documents may come from teaching and research institutions in France or abroad, or from public or private research centers.

L'archive ouverte pluridisciplinaire **HAL**, est destinée au dépôt et à la diffusion de documents scientifiques de niveau recherche, publiés ou non, émanant des établissements d'enseignement et de recherche français ou étrangers, des laboratoires publics ou privés.

Journal of Applied Physics

# Vertical breakdown of GaN on Si due to V-pits

Cite as: J. Appl. Phys. **127**, 015701 (2020); https://doi.org/10.1063/1.5129248
Submitted: 26 September 2019 . Accepted: 16 December 2019 . Published Online: 06 January 2020

S. Besendörfer, E. Meissner, A. Tajalli, M. Meneghini, J. A. Freitas, J. Derluyn, F. Medjdoub, G. Meneghesso, J. Friedrich, and T. Erlbacher

COLLECTIONS

Paper published as part of the special topic on Defects in Semiconductors 2020 DIS2020

F This paper was selected as Featured

View Online Export Citation CrossMark

ARTICLES YOU MAY BE INTERESTED IN

Direct detection of rare earth ion distributions in gallium nitride and its influence on growth morphology
Journal of Applied Physics **127**, 013102 (2020); https://doi.org/10.1063/1.5134050

Methodology for the investigation of threading dislocations as a source of vertical leakage in AlGaN/GaN-HEMT heterostructures for power devices
Journal of Applied Physics **125**, 095704 (2019); https://doi.org/10.1063/1.5065442

Transmorphic epitaxial growth of AlN nucleation layers on SiC substrates for high-breakdown thin GaN transistors
Applied Physics Letters **115**, 221601 (2019); https://doi.org/10.1063/1.5123374

© 2020 Author(s).

Journal of Applied Physics | ARTICLE | scitation.org/journal/jap

# Vertical breakdown of GaN on Si due to V-pits

Cite as: J. Appl. Phys. **127**, 015701 (2020); doi: 10.1063/1.5129248
Submitted: 26 September 2019 · Accepted: 16 December 2019 ·
Published Online: 6 January 2020

View Online Export Citation CrossMark

S. Besendörfer,[1,a)] E. Meissner,[1,2] A. Tajalli,[3] M. Meneghini,[3] J. A. Freitas, Jr.,[4] J. Derluyn,[5] F. Medjdoub,[6] G. Meneghesso,[3] J. Friedrich,[1] and T. Erlbacher[1,2]

## AFFILIATIONS

[1]Fraunhofer Institute for Integrated Systems and Device Technology IISB, Schottkystr. 10, 91058 Erlangen, Germany
[2]Chair of Electron Devices, University of Erlangen-Nürnberg, Cauerstr. 6, 91058 Erlangen, Germany
[3]Department of Information Engineering, University of Padova, via Gradenigo 6/B, 35131 Padova, Italy
[4]Naval Research Laboratory, 4555 Overlook Avenue, Washington, DC 20375, USA
[5]EpiGaN, Kempische Steenweg 293, 3500 Hasselt, Belgium
[6]CNRS-IEMN, Institute of Electronics, Microelectronics and Nanotechnology, Avenue Poincaré, 59650 Villeneuve d'Ascq, France

**Note:** This paper is part of the Special Topic on Defects in Semiconductors 2020.
[a)]**Author to whom correspondence should be addressed:** sven.besendoerfer@iisb.fraunhofer.de

## ABSTRACT

Gallium nitride on silicon (GaN/Si) is an important technological approach for power electronic devices exhibiting superior performance compared to devices based on a pure silicon technology. However, the material defect density in GaN/Si is high, and identification of critical defects limiting device reliability is still only partially accomplished because of experimental difficulties. In this work, atomic force microscopy, scanning electron microscopy, secondary ion mass spectrometry, and cathodoluminescence were employed to investigate commonly occurring epitaxial overgrown V-pits and inhomogeneous incorporation of oxygen and carbon across layer stacking in the vertical direction. These experiments identified V-pits as regions with higher n-type carrier concentrations and paths for vertical leakage through the buffer, as directly probed by conductive atomic force microscopy. The deleterious effect of V-pits on device performance is demonstrated by evaluating test devices fabricated on two wafers with significantly diverse density of buried V-pits induced by varying growth conditions of the aluminum nitride nucleation layer. A clear correlation between observed vertical breakdown and density of V-pits within the C-doped GaN layer below the device structures is obtained. Back-gating transient measurements also show that the dynamic device behavior is affected by the V-pit density in terms of the detrapping time constants.

*© 2020 Author(s). All article content, except where otherwise noted, is licensed under a Creative Commons Attribution (CC BY) license (http://creativecommons.org/licenses/by/4.0/).* https://doi.org/10.1063/1.5129248

## I. INTRODUCTION

Commercially available and state-of-the-art nitride-based power electronic devices are high electron mobility transistors (HEMTs) based on AlGaN/GaN heterojunctions.[1,2] High price, limited dimension, and commercial availability of native GaN substrates compel the use of foreign substrates for device fabrication. Low cost, high crystalline quality, and large diameter wafer availability promote Si as a potential substrate for the growth of AlGaN/GaN heterostructures. However, in that case, a complex buffer layer structure needs to be grown first in order to mitigate strain caused by lattice and thermal expansion coefficient mismatch as well as to reduce the ingrown defect density and related vertical leakage current. In fact, this is physically only possible to a certain extent, and consequently, device performance and reliability remain below the theoretically achievable material limits. An important step forward that is still only partially made up to date would be the clear identification of most critical defects and their role with regard to crucial device parameters, e.g., the vertical breakdown of gallium nitride on silicon (GaN/Si). According to the aimed device application, this would help to focus on the reduction of certain defects during the fabrication of a device structure allowing to push the performance toward the expected limit.[3] This is a very difficult experimental task considering that every device contains simultaneously many different types of defects. The most prominent defects are dislocations. Although there is no direct experimental evidence, they are often assumed


© Author(s) 2020

to be responsible for an early breakdown of GaN/Si.[4] Dislocations have been shown to act as vertical leakage paths and to have an impact on reverse bias leakage of Schottky diodes.[5–10] Another very common type of defect is the so-called V-pit.[10–16] V-pits are extended defects that are buried inside the buffer for the case of epitaxial structures and usually do not form any characteristic features on the sample surface,[10] which makes them very challenging to observe. V-pits are widely discussed in the field of optoelectronics because they influence the efficiency of light emitting diodes (LEDs), especially discussed for green LEDs.[12] However, their impact in the case of power electronic devices such as AlGaN/GaN HEMTs is rarely discussed. It has been shown that V-pits might promote vertical leakage and breakdown, but there was no direct evidence that leakage really occurs at V-pit sites and dominates over leakage caused by dislocations or dislocation bundles.[10,13,14] Moreover, a correlation between V-pits and premature vertical breakdown was only performed for structures with a surface covered by open V-pits, which is a different case compared to a material that is optimized in terms of interface roughness and that is used in commercial devices. In this work, we identify and demonstrate that buried V-pits are critical defects in GaN/Si. It is shown that they act as strong leakage current paths, dominating over leakage through dislocations, and have a strong impact on device breakdown. The microstructural supporting evidence of this observation is revealed, and the consequence for the premature vertical breakdown of a device is demonstrated by a combination of several techniques with statistical analysis of defect content and device performance. It turns out that the C-doped GaN-buffer layer is very sensitive to the amount of ingrown V-pits in terms of electrical robustness and that observed differences in the breakdown cannot be related to differences in near-surface dislocation density or sample topography.

## II. EXPERIMENTAL DETAILS

Two AlGaN/GaN-HEMT heterostructures grown by metal organic chemical vapor deposition (MOCVD) on 6 inch diameter p-doped Si(111) are investigated in this study and are named sample A and B in the following. Both of them were deposited under the same conditions and have identical layer structures and thicknesses, with the exception of the initial AlN nucleation layer [see Fig. 1(a)]. The growth conditions of this first layer were varied in terms of temperature, where the nucleation for sample B was optimized as compared to sample A as proposed by Freedsman *et al.*[17] The resulting difference in AlN layer morphology was intended to give a significant imprint on structural and potentially electrical characteristics of layers grown on top, i.e., specifically on internal V-pit density. The subsequent buffer layers consist of step-graded AlGaN layers with decreasing Al-content toward the GaN layer (GaN:C) on top, which was doped by C with a concentration of $\sim 1 \times 10^{19}\,\mathrm{cm}^{-3}$. The channel layer is an unintentionally doped GaN layer (GaN:uid), which is followed by an AlGaN-barrier and an *in situ* grown SiN-cap. Isolated Ohmic contacts of different sizes were deposited on both samples for electrical measurements. They consist of Ti/Al/Ni/Au stacks, annealed at 875 °C. Isolation around the contacts was performed by N-implantation. Vertical breakdown of the material was determined by on-wafer measurements, and ramping up the applied bias until a hard breakdown occurred.

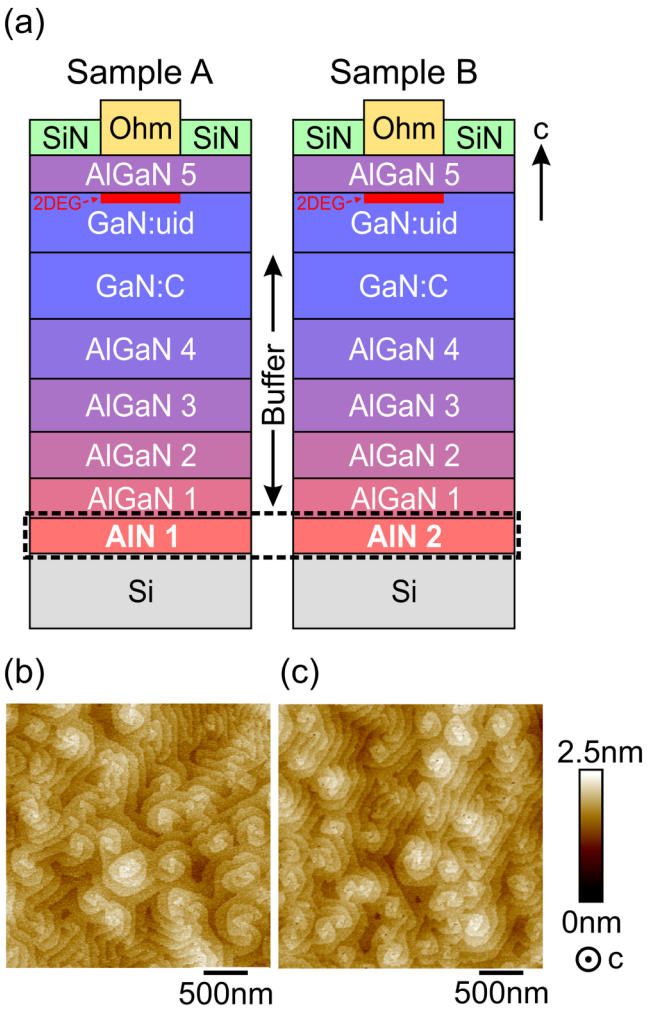


**FIG. 1.** (a) Layer structures of samples A and B were grown under identical conditions with the exception of the AlN nucleation layer (highlighted by the dashed line). For vertical breakdown measurements, isolated Ohmic contacts were processed. The topography of the AlGaN layer after removal of SiN is shown in (b) for sample A and in (c) for sample B.

Back-gating current transient measurements were also performed on these wafers. Sample preparation in terms of cross sectioning and fabrication of slanted samples was done by dicing and mechanical polishing. Cathodoluminescence (CL) measurements were carried out using a Gatan MonoCL3 system attached to a Jeol JSM-7500F Scanning Electron Microscope (SEM). Investigations by Energy Dispersive X-Ray Spectroscopy (EDS) were carried out with an X-Max Detector from Oxford Instruments also attached to the abovementioned SEM. Secondary Ion Mass Spectrometry (SIMS) was used in order to obtain quantitative depth profiles of impurity element traces. The spot size for these measurements was $150 \times 150\,\mu\mathrm{m}^2$, but only the central $50 \times 50\,\mu\mathrm{m}^2$ was used for analysis to minimize edge artifacts. Vertical leakage current mappings


© Author(s) 2020

were performed with Conductive Atomic Force Microscopy (C-AFM) fitted with boron-doped diamond-coated Si-tips, by applying a bias between the AFM-tip and Si substrate with the tip being grounded. The C-AFM and AFM measurements in the tapping mode were performed with a Bruker Dimension Icon. Defect Selective Etching (DSE) in KOH/NaOH eutectic melt at 450 °C for 4 min was used for revealing the near-surface dislocation structure.

## III. RESULTS AND DISCUSSION

### A. Device characteristics

Vertical breakdown measurements were carried out on isolated Ohmic contacts of different sizes on both samples [Fig. 2(a)]. The mean voltages of the hard breakdown of sample A are generally lower for all contact sizes compared to those of sample B [Fig. 2(b)]. As layer structures are identical, this observation is indicative of different densities of electrically active defects within the buffer. They seem to have their incorporation in the initial nucleation layer, considering that this is the only difference between the two samples. Accordingly, sample A is expected to have a much higher density of such defects. Another striking feature is the dependency of breakdown on contact size. This supports the idea that breakdown is sensitive to the specific amount of these defects below the corresponding contact. The dependency seems not to be linear because sample A shows a much less pronounced correlation of breakdown with respect to the device area than sample B. The inhomogeneity of the material and its electrical properties seem to correlate with the wide range of observed

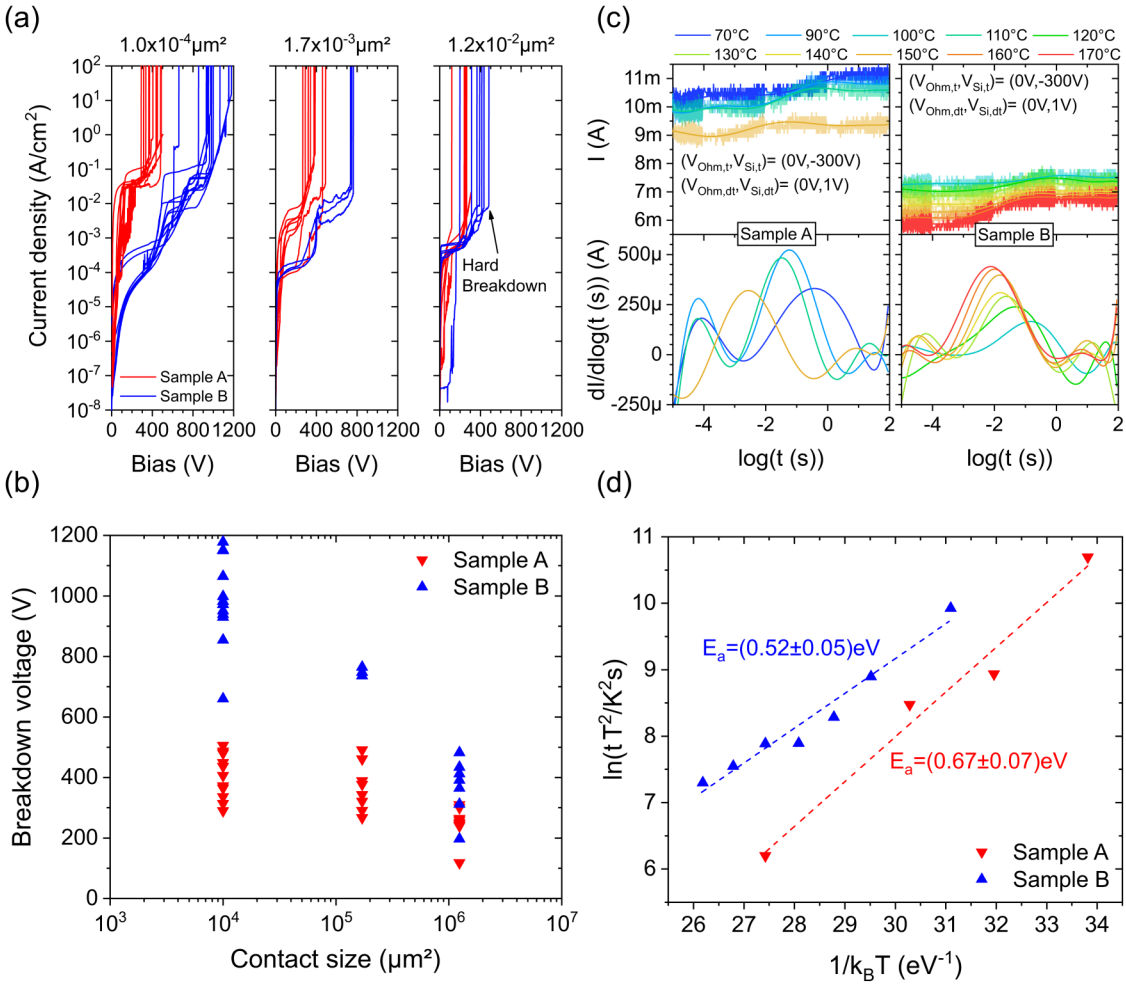


**FIG. 2.** (a) Hard vertical breakdown of both samples measured on contacts of different sizes. (b) The mean breakdown voltages obtained from (a) decrease strongly with increasing contact size for sample B, but only weakly for sample A. (c) Back-gating measurements of the detrapping current transients. (d) Arrhenius plot of the main detrapping time constants from (c). The activation energies obtained from linear fittings are comparable, but the time constants are smaller for sample A, which is indicative of a leaky buffer.


© Author(s) 2020

breakdown values on each contact size. Electrical properties of the buffer can also be probed by back-gating transient measurements.[18,19] For this experiment, Ohmic contacts of $100 \times 100\,\mu m^2$ deposited on both samples were used considering that the large difference on the breakdown measurements occurs for this contact size. In the trapping state, a potential of $V_{Si,t} = -300$ V was applied to the Si substrate and a potential of $V_{Ohm,t} = 0$ V to the Ohmic contact for 10 s. After switching to the detrapping state by applying a potential of $V_{Si,dt} = 1$ V to the Si substrate and a potential of $V_{Ohm,dt} = 0$ V to the Ohmic contact, detrapping characteristics were analyzed by monitoring the current transient for 100 s and extracting the most prominent detrapping time constant. This procedure was repeated for several temperatures between 70 °C and 170 °C for one device on each sample [Fig. 2(c)]. A linear fit of the obtained time constants in an Arrhenius plot yields the corresponding activation energy of the detrapping process [Fig. 2(d)]. A value of (0.67 ± 0.07) eV is found for sample A, which was identified to correspond to C or O impurities,[20] $N_{Ga}$,[21,22] or $V_N$.[23] For sample B, the observed activation energy is (0.52 ± 0.05) eV, related to C or O impurities[24] or to $N_{Ga}$.[21,22] For both samples, the errors of the slopes of the fitted lines were assumed to represent the uncertainty of the activation energy. The linear fits are shifted relative to each other in a way that sample A exhibits detrapping time constants that are a factor of 5–10 lower compared to sample B, over the entire temperature range. A general faster detrapping can be explained by the presence of vertical leakage paths within the buffer.[25] Therefore, the back-gating transient measurements are in good agreement with the vertical breakdown results.

### B. Surface-near defects

Before analyzing the buffers in detail, the topography of both samples was characterized by AFM in the tapping mode after etching away the SiN-cap. It turned out that the surface roughness on a scale of $20 \times 20\,\mu m^2$ is 0.8 nm (rms value) for sample A and 1.0 nm for sample B [see Figs. 1(b) and 1(c)]. Only step-flow growth as well as little dislocation-induced depressions of around 20 nm in diameter and 0.5 nm in depth were detected. There is no hint for any extended defects. Dislocations have been reported to serve as vertical leakage current paths depending on their type, where threading screw dislocations (TSDs) and threading dislocations (TDs) of mixed type are consistently reported to be much more critical than threading edge dislocations (TEDs).[5–10] In addition, clustering of dislocations was considered to be critical for vertical device breakdown.[26] However, the role of single dislocations in GaN/Si with respect to vertical breakdown is unclear. As the dislocation content is sensitive to the nature of the nucleation layer,[27] we performed an investigation by DSE, which reveals the dislocation structure of the GaN:uid layer in the present work.[9] Similar total dislocation densities, $2.8 \times 10^9\,cm^{-2}$ for sample A and $2.1 \times 10^9\,cm^{-2}$ for sample B, were observed, while an identical TSD density of $6.8 \times 10^7\,cm^{-2}$ was verified for both samples. The small difference in total dislocation density is mainly due to TEDs. Moreover, no extensive difference in dislocation clustering could be observed. From these results, we conclude that the electrical behavior in terms of breakdown can neither be explained by the near-surface dislocation structure nor extended defects at the surface. However, the dislocation microstructure within the buffer was not explicitly studied in detail, which would be a matter of transmission electron microscopy and was not carried out in this present study.

### C. Nucleation and growth of V-pits

Cross sections of both samples have been prepared in order to investigate the buffer layers in detail. Figures 3(a) and 3(b) depict SEM images of the lower buffer regions of samples A and B. Both samples show overgrown V-pits emerging from the AlN nucleation layer. The observed line densities of cross-sectioned V-pits at the interface to the AlGaN1 layer are quite different: $8.4\,\mu m^{-1}$ for sample A and $2.8\,\mu m^{-1}$ for sample B. This results from different densities of nucleated AlN islands on the Si substrate, which form V-pits at their boundaries during lateral expansion growth. The opening angles of those V-pits are in the range between 60° and 80° for both samples, which corresponds to semipolar orientations. Such side-planes exhibit an atomic surface configuration that is N-rich compared to the pure Ga-polar c-planes. Overgrowth on such facets, for example, by subsequent AlGaN1-layer growth, results in smaller growth rates than overgrowth on c-facet, yielding an increase of the V-pit diameter at the growth front, as the growth proceeds. If this situation is maintained during the growth of several consecutive layers, a V-pit trace develops, propagating through the layer stack, and V-pits with increased diameter are

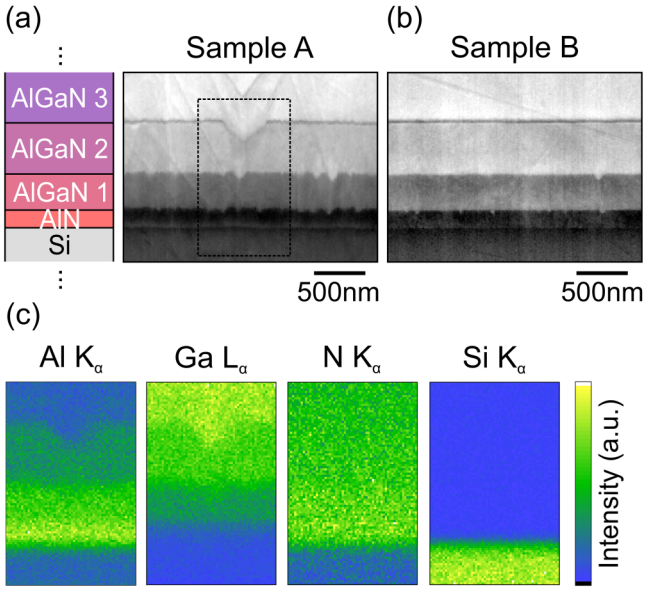


**FIG. 3.** Cross section of the lower buffer region of (a) sample A and (b) sample B observed by SEM. Sample A exhibits a higher density of overgrown V-pits, which can be seen at interfaces. For both samples, the V-pit density decreases toward the upper buffer region, but the V-pit diameter increases at the same time. In (c), EDS mappings of an overgrown V-pit like that marked in (a) are shown. No distinctive abnormalities in terms of elemental composition were observed within V-pit traces.


© Author(s) 2020

aligned vertically above each other at consecutive interfaces, as depicted in Fig. 3(a). Both samples show a decreasing V-pit density with increasing distance from the nucleation layer, but sample B consistently shows a much lower density than sample A in the upper buffer region. Note that highly developed V-pit traces reaching up to the GaN:C layer or even the GaN:uid layer are only observed in sample A.

### D. Impurity incorporation driven by V-pit overgrowth

Material of locally different doping levels and thus electrical properties can result from locally different growth conditions, for example, due to different surface terminations and resulting growth rates. Overgrowth of V-pits is a situation where such an effect can occur. Locally strong n-type doping in GaN/Si buffers was already observed in the past and was attributed to the presence of O in V-pits.[10] Figure 4 depicts the concentration depth profiles of major electrically relevant impurities (Si, C, and O) measured by SIMS. The Si-profiles of both samples are nearly identical, and the absolute values only vary between different layers. The O- and C-concentrations also vary between different layers and are known to depend on the Al-composition of the individual AlGaN layers.[29–31] Despite the fact that all equivalent AlGaN layers of the buffer were grown under the same conditions and exhibit an identical Al-content, as verified by EDS, significantly different O- and C-concentrations were observed in the lower buffer region. The mean O-concentration in AlGaN1 and AlGaN2 of sample A is near one order of magnitude higher than that of the corresponding two layers in sample B. In AlGaN3, the difference is only around

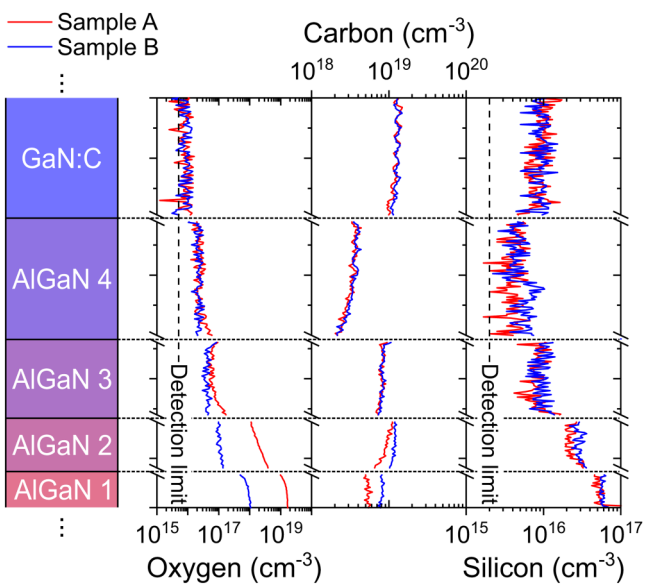


**FIG. 4.** SIMS depth profiles of all electrically relevant impurities. For O and C, significant differences between both samples could be observed within equivalent layers in the lower buffer region. Sample A shows a higher O-, but lower C-concentration there.

50% and identical in the layers above. In contrast, the mean C-concentration in AlGaN1 and AlGaN2 of sample A is up to 50% lower than that in sample B and identical in all layers above. Considering that SIMS measurements only give an idea about the depth dependence of impurity concentrations within a $50 \times 50\,\mu m^2$ column through the layer stack, CL imaging was used to obtain a much better spatially resolved probing technique. Figure 5(a) shows a typical cross-sectional SEM image of a highly developed V-pit trace within sample A. Figure 5(b) depicts the corresponding panchromatic CL-image recorded with 4 keV beam energy at room temperature at the same location. Along the V-pit trace, which means within the region of overgrowth, strong luminescence intensity up to 1.5 orders of magnitude higher than that at the surrounding material was detected. However, the luminescence intensity within the V-pit trace is very inhomogeneous, including at the sub-100 nm scale. As a consequence, drift makes a selective spectroscopic study at higher spectral resolution and a good signal-to-noise ratio difficult. Despite that, quickly measured point spectra with a spectrometer bandpass of 11 nm could be recorded with 4 keV beam energy at room temperature, within and outside of the V-pit trace, in GaN:C-, AlGaN4-, and AlGaN3 layers, as represented in Fig. 6(a). Two main emission bands are observed in all spectra: the near band edge emission (NBE) at higher energy and the blue luminescence (BL) at lower energy regions of the recorded spectra. As expected, both the positions of the NBE and the BL shift to higher energy with increasing Al-content.[32] However, the NBE measured within the V-pit trace is much more intense than that observed in the surrounding area and exhibits an inhomogeneous broadening most likely due to the contribution from various recombination processes. The strong NBE intensities within the V-pit trace compared to nearby regions, highlighted in Fig. 5(c), were observed by monochromatic CL-mappings using a spectrometer bandpass of 11 nm. Locally enhanced NBE intensity in n-type GaN or AlGaN may result from locally higher shallow donor concentrations[33] due to incorporation of O and Si in the form of $O_N$ and $Si_{Ga}$, respectively,[35,36] or from locally lower concentrations of nonradiative and/or compensating centers related to C such as $C_N$.[34,37] A lower C-concentration within the V-pit trace can also lead to a reduced BL,[26,34] which is observed in Fig. 6(a) as well as in the monochromatic mapping of the AlGaN3-BL with a spectrometer bandpass of 11 nm represented in Fig. 5(d). A temperature-dependent study of the NBE within V-pit traces and surrounding regions was obtained from slanted samples, which were prepared by cutting a sample along a plane tilted by 5° against the c-plane, as shown in Fig. 7(a). First, two suitable areas for investigation were selected at the AlGaN4 layer: an area free of V-pits [CL1 in Fig. 7(a)] and an area containing a V-pit trace [CL2 in Fig. 7(a)]. Second, CL-spectra integrated over both areas were recorded for a set of several temperatures with a spectrometer bandpass of 2 nm. As both areas were selected far from the interface with the AlGaN3 layer, no signal contribution from this layer is expected for spectra acquired with a beam energy of 5 keV. This procedure results in two sets of spectra: one set shows the temperature-dependent NBE of a V-pit free area of the AlGaN4 layer [pure layer spectra, Fig. 6(b)] and the other set, the temperature-dependent NBE of an area containing a V-pit. For each temperature, the pure layer spectrum was subtracted from the mixed spectrum in order to obtain a spectrum of the pure V-pit


© Author(s) 2020

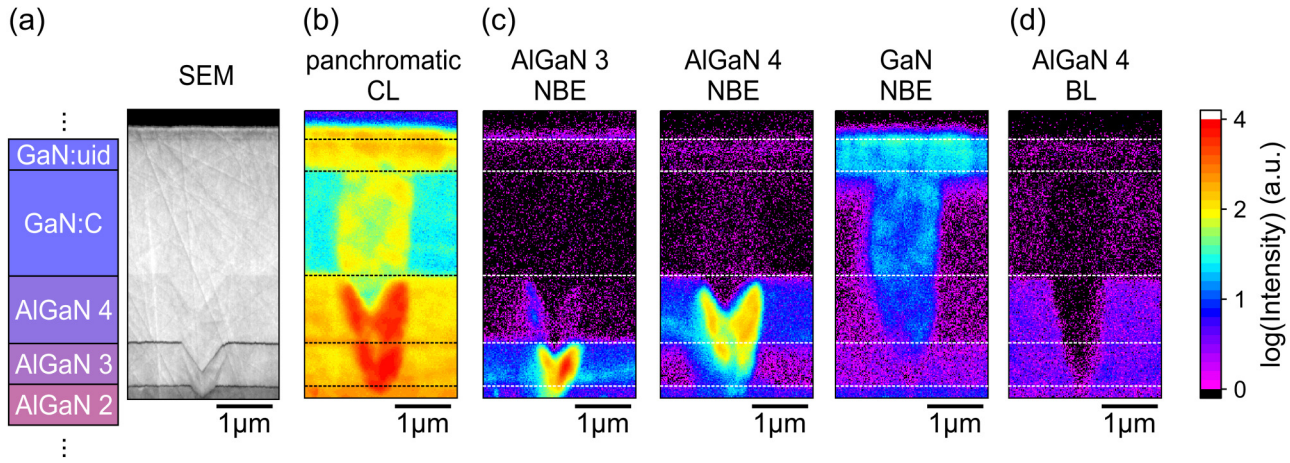


**FIG. 5.** (a) SEM image of a cross-sectioned V-pit trace and (b) the corresponding panchromatic CL-mapping. In (c), the monochromatic mappings (spectrometer bandpass 11 nm) at the energy positions of the NBE emission bands of AlGaN3, AlGaN4, and GaN [see also Fig. 6(a)] are shown. (d) Monochromatic mapping at the energy position of the BL of AlGaN4, which also shows the BL of AlGaN3 and GaN:C at the same time due to the used spectrometer bandpass of 11 nm [see also Fig. 6(a)].

related signals [Fig. 6(b)]. All V-pit spectra consist of at least two bands. For further analysis, the V-pit spectra were fitted by a sum of two Gaussian lines and the layer spectra by a single Gaussian line. The peak positions of the V-pit free region spectra nearly shift linearly to lower energies with increasing temperature over the whole investigated range [Fig. 6(c)]. The peak positions of the two V-pit related emission bands shift to lower energies with increasing temperature only for temperatures above 176 K [Fig. 6(c)] and are generally shifted to lower energies with respect to the single band of the V-pit free region spectra. This shift is not due to local variations in Al-composition as verified by EDS [Fig. 3(c)] and unlikely due to strain only because the observed shifts are much larger than expected.[38,39] We assume the involvement of a different defect such as a deeper and/or metastable center involving Si, O, vacancies, or V-impurity complexes. The integrated peak intensities of the two V-pit emission bands show stronger dependence on temperature than that of the V-pit free spectra [Fig. 6(d)]. In addition, the ratio of the integrated intensity Band2/Band1 also increases with increasing temperature, indicating different activation energies. These observations are indicative for different defect types and concentrations within the V-pit traces compared to their surrounding region. The results from CL and SIMS consistently indicate that the observed differences in O- and C-concentration in the lower buffer region are mainly related to different V-pit densities and that overgrowth of V-pits leads to increased O- and reduced C-incorporations. Under the assumption of "ideal" crystallographic surface terminations and comparable growth rates of the semipolar plane and c-plane, this hypothesis is supported by the study of Cruz *et al.*[28] However, as discussed above, observed V-pit traces develop due to a slower growth rate of semipolar planes meaning that growth conditions are not comparable and, therefore, might play a significant role as well. The observation of comparable concentrations of O and C in the upper buffer region does not imply that the V-pit densities in both samples are similar. This might be related to mainly two facts; first, the corresponding total V-pit concentration is too low in the upper buffer and the SIMS-spot cannot detect their contribution to the O- or C-incorporation; second, the O-incorporation into V-pit traces might be less pronounced in Al-poor AlGaN layers compared to Al-rich layers.

### E. V-pit traces as vertical leakage paths

The consequences of enhanced O- and reduced C-concentrations inside the V-pit traces with respect to electrical properties were directly probed by C-AFM. The slanted sample was used again, and the exact locations of a specific set of V-pits were identified by panchromatic CL-mappings by recording spotlike bright luminescence [Fig. 7(b)]. Simultaneously obtained SEM images often show a hexagonal area of a slightly higher secondary electron intensity at the position of cut V-pit traces, which corresponds to a smaller work function of the material or higher n-doping [Fig. 7(c)]. The selected area was then mapped by C-AFM with a potential of −10 V applied to the Si substrate with the AFM-tip being grounded. The obtained current map represents the vertical leakage through the underlying buffer structure and exhibits discrete spots of strong leakage current at the positions of V-pits [Fig. 7(d)], whereas the background leakage beside the V-pits is within the noise level of the setup. This result directly shows that V-pit traces act as vertical leakage current paths in the buffer at low voltages. This is in agreement with the results from back-gating measurements, which showed that sample A might exhibit a higher density of vertical leakage paths in the buffer. V-pits traces are, therefore, a potentially critical defect associated with premature vertical breakdown and might be as well the explanation for the observed behavior of breakdown highlighted in Fig. 2(a).

### F. Vertical breakdown driven by V-pits

The V-pit density of both samples was estimated assuming its dependence on the distance from the nucleation layer. For AlN-,


© Author(s) 2020

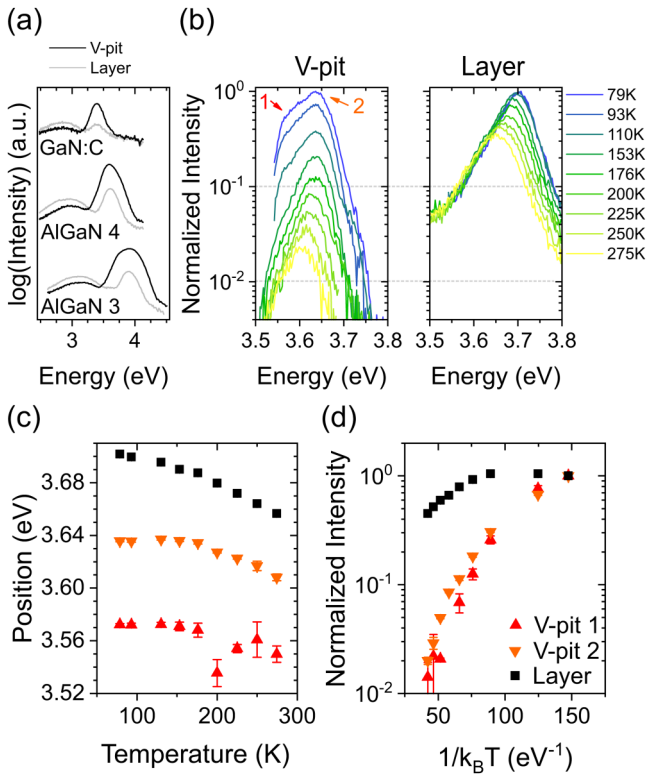


**FIG. 6.** (a) Point spectra recorded at random positions in AlGaN3, AlGaN4, and GaN:C within the V-pit trace shown in Fig. 5 and beside it in the layer with a spectrometer bandpass of 11 nm. (b) Temperature-dependent behavior of the NBE measured inside V-pit traces and outside with a spectrometer bandpass of 2 nm (for details, see text). The V-pit NBE consists of at least two emission bands (marked by 1 and 2). In (c), the temperature-dependent positions of the two resolved emission bands are shown together with the position of the NBE of the layer. Equivalently, the temperature dependence of the normalized, integrated intensity is shown in (d).

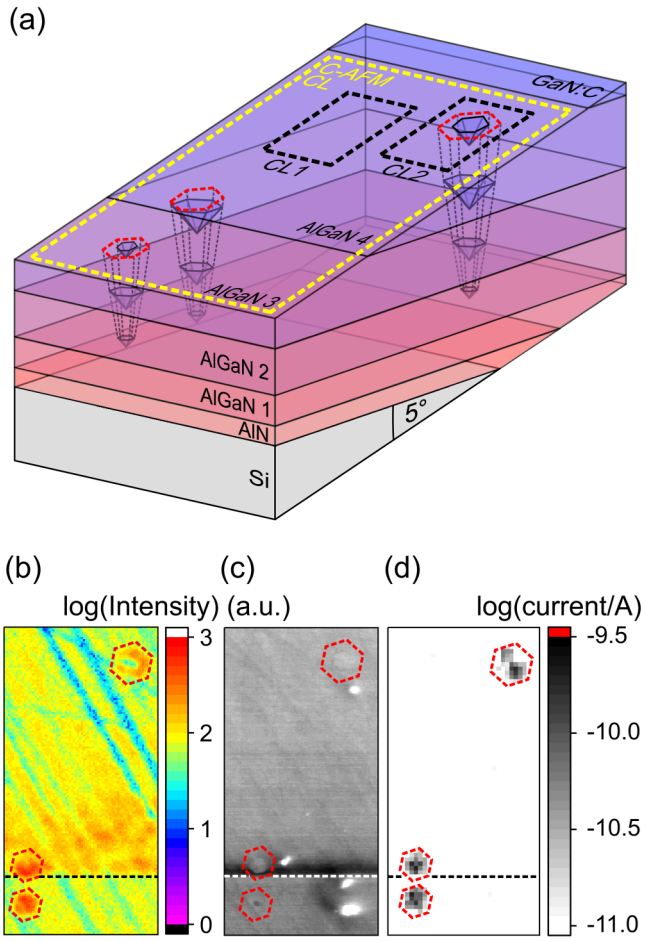


**FIG. 7.** (a) Geometry of the prepared slanted sample used for C-AFM and temperature-dependent CL measurements. In (b), a panchromatic CL-mapping of the area marked in yellow in (a) shows V-pit traces as bright spots that correspond to hexagonal contrasts in the corresponding SEM image in (c). (d) A C-AFM mapping of the same area as shown in (b) and (c) reveals strong spots of vertical leakage at the positions of V-pit traces.

AlGaN1-, and AlGaN2 layers, this was achieved by counting the number of V-pits along a line of several 10 $\mu$m at the upper interfaces of these layers by cross-sectional SEM. The resulting line density was then divided by the estimated mean diameter of V-pits at these interfaces. This procedure could not be used in the upper buffer due to its much lower V-pit density. Hence, the densities were estimated by counting the amount of CL luminescence spots measured on the slanted samples. An error of 50% was assumed for all estimated density values. The result is depicted in Fig. 8(a). Sample A starts with a V-pit density of $2.1 \times 10^{10}\,\mathrm{cm}^{-2}$ in the nucleation layer, which drops in the upper buffer region to a density of $10^6 - 10^7\,\mathrm{cm}^{-2}$, yielding a decrease of 3–4 orders of magnitude. Within each layer of the upper buffer, the density is fairly constant with the exception of the GaN:C layer, where closing of V-pits occurs. Sample B starts with a V-pit density of $6.9 \times 10^9\,\mathrm{cm}^{-2}$ in the nucleation layer, which drops to only $10^3 - 10^5\,\mathrm{cm}^{-2}$ in the upper buffer, which is 2–3 orders of magnitude less than in the equivalent layers of sample A. In the AlGaN4 and GaN:C layer of sample B, no V-pits could be observed at all. For GaN:C, a value of $1 \times 10^4\,\mathrm{cm}^{-2}$ was extrapolated, but the assumed real value is expected to be in the range between $1 \times 10^3\,\mathrm{cm}^{-2}$ and $5 \times 10^4\,\mathrm{cm}^{-2}$, as indicated by the error bars. A correlation of V-pits and the observed values of vertical breakdown is carried out by comparing the mean values of the vertical breakdown of each contact size on both samples with the statistically expected mean amount of underlying V-pits at the upper surface of GaN:C [Fig. 8(b)]. As the V-pit density at this location in sample B is only extrapolated, the corresponding calculated numbers of V-pits reach large uncertainties, whereas all other values maintain their error of 50%. GaN:C is chosen for this correlation because this layer is known to be especially critical with regard to vertical robustness.[40,41] V-pits at the upper surface of the GaN:C layer are characteristic for underlying V-pit traces that


© Author(s) 2020

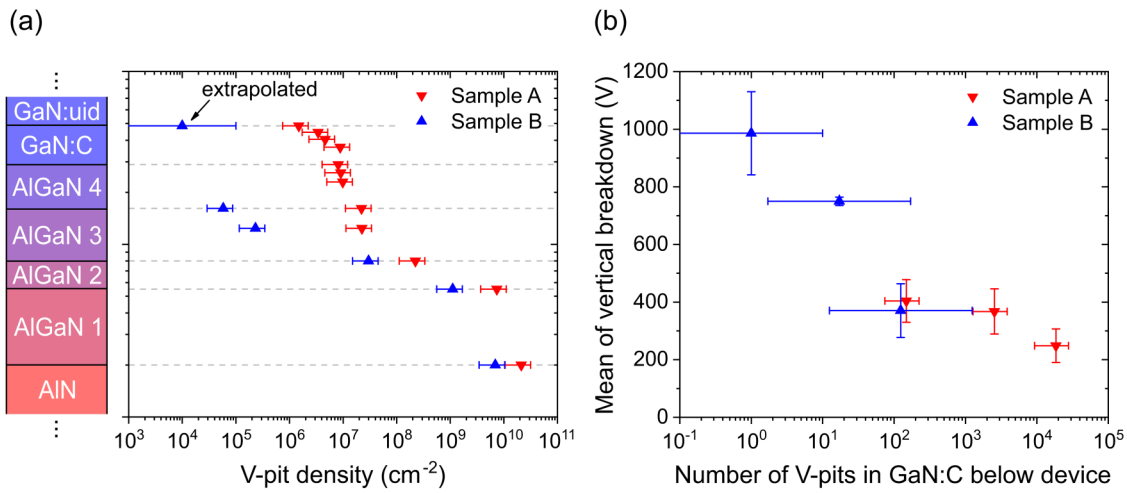


**FIG. 8.** (a) V-pit density in dependence of the depth within both samples. The obtained values for the surface of GaN:C are used to calculate the statistically expected amount of V-pits at this position underneath the Ohmic contacts that were investigated in Fig. 2. The mean breakdown plotted against those values is shown in (b). A logarithmic dependence is obtained for breakdown values between 300 V and 1000 V. Higher breakdown values might not be achieved due to V-pits deeper in the structure or due to other defects such as dislocations.

penetrate the whole buffer downwards [see also Fig. 5(b)]. A logarithmic dependence of the breakdown on the number of V-pits is obtained, which is in good agreement with the prior evaluation of correlation to open V-pits on the sample surface.[13] The analysis shows that below the smallest investigated contact area on sample B, there is only around one V-pit expected on average. The highest measured breakdown voltage of slightly below 1200 V is assumed to be observed on Ohmic contacts without any underlying V-pits in GaN:C. A value of 1200 V is in good agreement with nowadays achieved vertical breakdown voltages of state-of-the-art commercial GaN/Si device structures that are optimized in terms of their nucleation layer. Higher breakdown values might not be achieved due to the presence of V-pits located deeper in the buffer or by other defects such as dislocations. The causal relationship between directly observed vertical leakage current paths through the buffer due to V-pits and the statistically found role of V-pits in terms of vertical breakdown might be one of the following or a combination of them: (i) thermal runaway due to a locally high leakage current through V-pits in the buffer; (ii) defect percolation process locally favored by high electric field and/or leakage current, where an enhanced electric field might be induced by the sharp geometry of V-pits at their lower side; and (iii) a fast electromigration process that induces metal moving into the cores of TDs directly below the V-pits.

## IV. CONCLUSION

In conclusion, we present the first study directly showing that overgrown V-pits in GaN/Si act as vertical leakage paths through the buffer, which is detrimental to power devices. In addition, a clear correlation between the amounts of overgrown buried V-pits within the device insulating C-doped GaN layer and the premature vertical breakdown was explicitly found and discussed. The surface-near dislocation structure is shown to have no dominant effect in our case and for our investigated breakdown voltages. As C-AFM measurements only showed vertical leakage paths associated with V-pit traces, we assume that there is also no dominant role of the dislocation structure in the buffer. The major effect explaining the leakage as well as the vertical breakdown stems from the V-pits penetrating through the buffer into the GaN:C layer and degrading its electrical insulation performance, which can be expressed semiquantitatively by the total number of V-pits correlated with the breakdown of devices. Our work points out the importance of a well coalesced nucleation layer that is indispensable in order to shift the material performance toward its physical limit. Our results make an important contribution not only to growth optimization, but also to metrological and, therefore, device yield related aspects. An *ex situ*, full wafer mapping of the V-pit distribution within the upper buffer region might be addressed by interface roughness mapping using X-Ray based methods, which may allow a better understanding of transistor reliability. A low interface roughness can be monitored *in situ* by optical methods such as laser reflectance. As V-pits are also a prominent defect in GaN-wafers grown by hydride vapor phase epitaxy (HVPE), our work is also relevant for reliability aspects of the potentially upcoming future technology of commercially available GaN/HVPE-GaN power devices.

## ACKNOWLEDGMENTS

This work was carried out within the project InRel-NPower, which has received funding from the European Union's Horizon 2020 research and innovation program under Grant Agreement No. 720527. J. A. Freitas, Jr., was supported by the Office of Naval Research (ONR). The authors would like to thank M. Müller for performing parts of the AFM measurements and O. Krause from Nanoworld GmbH for supporting AFM-related work.


© Author(s) 2020

## REFERENCES


[1]O. Ambacher, J. Smart, J. R. Shealy, N. G. Weimann, K. Chu, M. Murphy, W. J. Schaff, L. F. Eastman, R. Dimitrov, L. Wittmer, M. Stutzmann, W. Rieger, and J. Hilsenbeck, J. Appl. Phys. **85**, 3222 (1999).
[2]M. Meneghini, G. Meneghesso, and Z. Enrico, *Power GaN Devices* (Springer International Publishing, Cham, 2017).
[3]G. Meneghesso, J. Derluyn, E. Meissner, F. Medjdoub, A. Banerjee, J. Naundorf, and M. Rittner, Bodo's Power Syst., 52–55 (August 2018).
[4]A. Dadgar, T. Hempel, J. Bläsing, O. Schulz, S. Fritze, J. Christen, and A. Krost, Phys. Status Solidi C **8**, 1503–1508 (2011).
[5]J. W. P. Hsu, M. J. Manfra, D. V. Lang, S. Richter, S. N. G. Chu, A. M. Sergent, R. N. Kleiman, L. N. Pfeiffer, and R. J. Molnar, Appl. Phys. Lett. **78**, 1685 (2001).
[6]J. W. P. Hsu, M. J. Manfra, R. J. Molnar, B. Heying, and J. S. Speck, Appl. Phys. Lett. **81**, 79 (2002).
[7]B. S. Simpkins, E. T. Yu, P. Waltereit, and J. S. Speck, J. Appl. Phys. **94**, 1448 (2003).
[8]B. Kim, D. Moon, K. Joo, S. Oh, Y. K. Lee, Y. Park, Y. Nanishi, and E. Yoon, Appl. Phys. Lett. **104**, 102101 (2014).
[9]S. Besendörfer, E. Meissner, A. Lesnik, J. Friedrich, A. Dadgar, and T. Erlbacher, J. Appl. Phys. **125**, 095704 (2019).
[10]M. Moseley, A. Allerman, M. Crawford, J. J. Wierer, M. Smith, and L. Biedermann, J. Appl. Phys. **116**, 053104 (2014).
[11]F. S. Choi, J. T. Griffiths, C. Ren, K. B. Lee, Z. H. Zaidi, P. A. Houston, I. Guiney, C. J. Humphreys, R. A. Oliver, and D. J. Wallis, J. Appl. Phys. **124**, 055702 (2018).
[12]S. Zhou, X. Liu, H. Yan, Y. Gao, H. Xu, J. Zhao, Z. Quan, C. Gui, and S. Liu, Sci. Rep. **8**, 11053 (2018).
[13]S. L. Selvaraj, T. Suzue, and T. Egawa, Appl. Phys. Express **2**, 111005 (2009).
[14]M. Charles, Y. Baines, S. Bos, R. Escoffier, G. Garnier, J. Kanyandekwe, J. Lebreton, and W. Vandendaele, J. Cryst. Growth **464**, 164–167 (2017).
[15]E. Richter, M. Gründer, C. Netzel, M. Weyers, and G. Tränkle, J. Cryst. Growth **350**, 89–92 (2012).
[16]V. Voronenkov, N. Bochkareva, R. Gorbunov, P. Latyshev, Y. Lelikov, Y. Rebane, A. Tsyuk, A. Zubrilov, and Y. Shreter, Jpn. J. Appl. Phys. **52**, 08JE14 (2013).
[17]J. J. Freedsman, A. Watanabe, Y. Yamaoka, T. Kubo, and T. Egawa, Phys. Status Solidi A **213**, 424–428 (2016).
[18]J. Joh and J. A. del Alamo, IEEE Trans. Electron Devices **58**, 132–140 (2011).
[19]D. Bisi, M. Meneghini, C. de Santi, A. Chini, M. Dammann, P. Brückner, M. Mikulla, G. Meneghesso, and E. Zanoni, IEEE Trans. Electron Devices **60**, 3166–3175 (2013).
[20]M. Tapajna, R. J. T. Simms, Y. Pei, U. K. Mishra, and M. Kuball, IEEE Electron Device Lett. **31**, 662–664 (2010).
[21]D. Haase, M. Schmid, W. Kürner, A. Dörnen, V. Härle, F. Scholz, M. Burkard, and H. Schweizer, Appl. Phys. Lett. **69**, 2525–2527 (1996).
[22]H. K. Cho, C. S. Kim, and C.-H. Hong, J. Appl. Phys. **94**, 1485–1489 (2003).
[23]S. S. Hullavarad, S. V. Bhoraskar, S. R. Sainkar, S. Badrinarayanan, A. B. Mandale, and V. Ganesan, Vacuum **55**, 121–126 (1999).
[24]M. Caesar, M. Dammann, P. Polyakov, P. Waltereit, W. Bronner, M. Baeumler, R. Quay, M. Mikulla, and O. Ambacher, in *2012 IEEE International Reliability Physics Symposium (IRPS)* (IEEE, 2012), pp. CD.6.1–CD.6.5.
[25]M. J. Uren, S. Karboyan, I. Chatterjee, A. Pooth, P. Moens, A. Banerjee, and M. Kuball, IEEE Trans. Electron Devices **64**, 2826–2834 (2017).
[26]M. Knetzger, E. Meissner, J. Derluyn, M. Germain, and J. Friedrich, Microelectron. Reliab. **66**, 16–21 (2016).
[27]N. Mante, S. Rennesson, E. Frayssinet, L. Largeau, F. Semond, J. L. Rouvière, G. Feuillet, and P. Vennéguès, J. Appl. Phys. **123**, 215701 (2018).
[28]S. C. Cruz, S. Keller, T. E. Mates, U. K. Mishra, and S. P. DenBaars, J. Cryst. Growth **311**, 3817–3823 (2009).
[29]S. T. Bradley, S. H. Goss, L. J. Brillson, J. Hwang, and W. J. Schaff, J. Vac. Sci. Technol. B **21**, 2558 (2003).
[30]G. Parish, S. Keller, S. P. DenBaars, and U. K. Mishra, J. Electron. Mater. **29**, 15–20 (2000).
[31]H. W. Jang, J. M. Baik, M.-K. Lee, H.-J. Shin, and J.-L. Lee, J. Electrochem. Soc. **151**, G536–G540 (2004).
[32]N. Nepal, M. L. Nakarmi, J. Y. Lin, and H. X. Jiang, Appl. Phys. Lett. **89**, 092107 (2006).
[33]M. Leroux, N. Grandjean, B. Beaumont, G. Nataf, F. Semond, J. Massies, and P. Gibart, J. Appl. Phys. **86**, 3721–3728 (1999).
[34]R. Armitage, Q. Yang, and E. R. Weber, J. Appl. Phys. **97**, 073524 (2005).
[35]W. Seifert, R. Franzheld, E. Butter, H. Sobotta, and V. Riede, Cryst. Res. Technol. **18**, 383–390 (1983).
[36]W. Götz, N. M. Johnson, C. Chen, H. Liu, C. Kuo, and W. Imler, Appl. Phys. Lett. **68**, 3144–3146 (1996).
[37]J. L. Lyons, A. Janotti, and C. G. van de Walle, Appl. Phys. Lett. **97**, 152108 (2010).
[38]J. T. Holmi, B. H. Bairamov, S. Suihkonen, and H. Lipsanen, J. Cryst. Growth **499**, 47–54 (2018).
[39]D. G. Zhao, S. J. Xu, M. H. Xie, S. Y. Tong, and H. Yang, Appl. Phys. Lett. **83**, 677–679 (2003).
[40]W. Z. Wang, S. L. Selvaraj, K. T. Win, S. B. Dolmanan, T. Bhat, N. Yakovlev, S. Tripathy, and G. Q. Lo, J. Electron. Mater. **44**, 3272–3276 (2015).
[41]S. Kato, Y. Satoh, H. Sasaki, I. Masayuki, and S. Yoshida, J. Cryst. Growth **298**, 831–834 (2007).



© Author(s) 2020